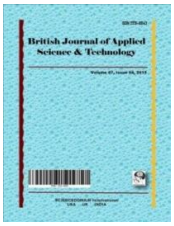

British Journal of Applied Science & Technology
20(1): 1-18, 2017; Article no.BJAST.30117
ISSN: 2231-0843, NLM ID: 101664541

SCIENCEDOMAIN *international*
www.sciencedomain.org

Geochemical Characterization and Protolith of the Migmatite-Gneisses of Tandama Area, Katsina State, NW Nigeria

Idzi O. Alaku[1*], Ogunbajo I. Moshood[1], Ako T. Agbor[1] and Alabi A. Amos[1]

[1]Department of Geology, Federal University of Technology Minna, Nigeria.

Authors' contributions

This work was carried out in collaboration between all authors. All authors read and approved the final manuscript.

Article Information

DOI: 10.9734/BJAST/2017/30117
Editor(s):
(1) Rares Halbac-Cotoara-Zamfir, Hydrotechnical Engineering Department, "Politehnica" University of Timisoara, Romania.
Reviewers:
(1) Kouankap Nono Gus Djibril, The University of Bamenda, Cameroon.
(2) Pavel Kepezhinskas, USA.
Complete Peer review History: http://www.sciencedomain.org/review-history/18566

Original Research Article

Received 18th October 2016
Accepted 27th February 2017
Published 10th April 2017

ABSTRACT

Migmatite-gneisses, which include migmatite, granite gneiss, and augen gneiss, underlie more than 70% of Tandama area, in North-western Nigeria. They are associated with schists, and are intruded by granites and pegmatites. These rocks are thought to have undergone a reworking during the Pan-African Orogeny. The aim of this research is to present results of geochemical investigation of Migmatite-gneiss Complex in the study area with a view to determine their geochemical characteristics and petrogenesis. Whole rock geochemical analyses have been used to evaluate the characteristics, petrogenesis and mode of emplacement of the protoliths. Geochemically, these rocks show granitic affinities. They are metaluminous to weakly peraluminous I-type, with S-type characteristic, magnesian to ferroan and alkali calcic and calcic. The protoliths could have been derived from the partial melting of tonalitic to granodioritic crustal rocks at low pressure, thus, producing metaluminous to slightly peraluminous high-silica, ferroan, alkali-calcic to calc-alkali melts, which is why it has some S-type character. These varying features are an indication that the protoliths are derived from mainly crustal melt mingled with mantle-derived component. The varying REEs and trace elements pattern displayed by the rocks is typical signature of arc rocks or continental crustal materials: the LREEs and LILE enrichment along with Rb, K, Pb, and negative Nb, Ta, Ti are evident of this signature. The incompatible trace elements

**Corresponding author: E-mail: idzioramealaku@gmail.com;*

show similarity to those of continental crustal rocks as indicated by the ratios in Th/U (2.21 – 12.4), Th/Yb (2.60 – 90.95), Ta/Yb (0.03 - 1.43), Ce/Pb (mainly 0.30 – 29.23) and high Ba/Nb (8.56 – 2402), the values of Sr/Y are generally<100, which is an indication of subduction-related rocks,the trend in Sr/Y ratio relative to Y contents in the rocks reflects essentially two types of felsic protolith namely crustal melts and slab melts. Similarly, the magnesian characteristic indicates close affinity to relatively hydrous, oxidizing melts, which is broadly typical of settings related to subduction. The high-K nature is characteristics of crustal rocks derived from remelting and differentiation of arc-accretionary complex crust. The rare earth element (REE) distribution shows that the migmatite-gneisses are enriched in the lighter rare earth elements (LREE) Sm, Pr, Nd, La and Ce, in that order of increasing abundance, with average values of 4.81 ppm, 7.90 ppm, 27.50 ppm, 38.44 ppm, 68.22ppm, respectively; and relatively depleted in the heavy rare earth elements (HREE) Lu, Tm, Tb, Ho, Yb and Er, with average values ranging 0.28 ppm, 0.30 ppm, 0.58 ppm, 0.65ppm, 1.91 ppm and 1.88 ppm respectively, and they exhibit negative EU anomaly, indicating that the rocks are highly fractionated. REE-chondrite normalized spider plot and plots in the chemical discrimination diagrams including the Y versus Nb plot, show that the protoliths were derived from partial melting and differentiation of granitic magma of hybrid origin which were emplaced in volcanic arc (VAG) to Syn-collision granite (Syn-COLG) tectonic setting. Variations thus, suggest igneous precursors for the migmatite-gneisses of this area, were derived from differing sources and depths.

Keywords: Migmatite-gneisses; pan-african orogeny; syncollision; igneous protolith; I-type.

1. INTRODUCTION

The Migmatite-gneiss complex of the study area is one of the four major petro-lithological units that constitute the Basement complex of Nigeria, which lies within the Pan-African mobile belt and sandwiched between the West African Craton and Congo Craton. It has intrusions of Younger Granites and coverings of Cretaceous and younger sediments. The Migmatite-Gneiss Complex is the most widespread of the component units in the Nigerian basement. It has a heterogeneous assemblage comprising migmatites, orthogneises, paragneisses, and a series of basic and ultrabasic metamorphosed rocks. Petrographic evidence indicates that the Pan-African reworking led to recrystallization of many of the constituent minerals of the Migmatite-Gneiss Complex by partial melting with majority of the rock types displaying medium to upper amphibolite facies metamorphism [1].

The Migmatite-Gneiss Complex of the study area is located in north-western part of Nigeria and has heterogenous assemblages of migmatites, gneiss and augen gneiss. Some authors have attributed the Migmatite-Gneiss Complex of Nigeria to be of sedimentary origin while others view them as rocks of igneous origin. According to Rahaman [2], the geochemical data available were insufficient to equivocally distinguish between sedimentary and igneous gneisses. Grant [3] on the basis of $^{87}Sr/^{86}Sr$ studies of the Ibadan granite gneiss supported an igneous origin while Burke et al. [4] argued that the granite gneiss were derived from isochemical metamorphism of a shale-graywacke sequence (a sedimentary origin). Onyeagocha [5] on the basis of field and geochemical evidence proposed an igneous origin by partial melting of crustal rocks for the granite gneisses of north-central Nigeria. Supportive of the igneous origin, are also works of Ekwere and Ekwueme [6]; Imeokparia and Emofurieta [7] while Freeth [8] support a sedimentary origin. Elueze and Bolarinwa [9], studies of the granite gneiss of Abeokuta area gives a wide range of Ba and Zr concentration, concluded that the gneisses were of igneous parentage but with sedimentary input. This made it difficult to propose a single mode of origin for the granite gneisses in the Nigerian basement due to their variable compositions from location to location [9].

Works done on the genetics of migmatite-gneisses are restricted to the south-western basement of Nigeria [9-15]. However, the gneisses of the Malumfashi schist belt where the study area is situated were earlier identified by McCurry [16] on the basis of petrography and not geochemistry, and were on a regional scale. These paper therefore present results of geochemical investigation of Migmatite-Gneiss Complex, around Tandaman area of north-western Nigeria, with a view to determine their geochemical characteristics and petrogenesis.

2. METHODOLOGY

Rock samples that were obtained from different locations were taken to the sample preparation

laboratory at the Department of Geology and Mining, University of Jos, to prepare the samples for whole-rock analysis and rock mineral analysis. The samples were broken into smaller pieces using geologic hammer so that they can be grinded easily in the pulveriser. The smaller fragments were crushed and reduced to powder using FRITSCH Pulverisette 7. The equipment has two grinding bowls and each of them has grinding steel balls which crush and rip apart the rock fragments while rotating for 30 minutes at 400 revolutions per minute (400 rpm). The powdered samples, pulverised to 85% passing 200 mesh, and measured to 5 g were transferred into labelled dispersing gloves for transportation to Acme laboratory at Vancouver, Canada, where the lithogeochemical analysis were carried out using X-ray fluorescence (XRF) and Inductively coupled plasma mass spectrometry (ICP-MS).

The major oxides concentrations (wt. %) in the samples were determined using X-ray fluorescence (XRF) method, following fusion with Lithium tetraborate ($LiBO_2$). In order to determine the loss on ignition (LOI), a predetermined amount of each sample was roasted. The major oxides concentrations were determined using the roasted samples by fusing them in a platinum-gold crucible with a commercial lithium tetraborate flux. The molten materials are then cast in a platinum mold to form glass discs which were then analysed by X-ray fluorescence (XRF) to determine the major constituents. These oxides include SiO_2, Al_2O_3, Fe_2O_3, CaO, MgO, Na_2O, K_2O, MnO, TiO_2, P_2O_5, and Cr_2O_3.

The trace elements were determined using Inductively Coupled Plasma Mass Spectrometry (ICP-MS) method. The powdered samples were mixed with Lithium metaborate/tetraborate ($LiBO_2/Li_2B_4O_7$) flux in platinum crucibles. These were then fused in a furnace. The resulting beads were dissolved in ACS grade nitric acid and analysed by Inductively Coupled Plasma Mass Spectrometry (ICP-MS) in parts per million (ppm).14 elements which include gold (Au) and some volatile elements which do not report in lithium metaborate/tetraborate digestion were analysed after digestion with modified Aqua Regia Solution of equal parts concentrated Hydrochloric acid (HCl), trioxonitrate (V) acid (HNO_3) and dihydrogen monoxide (DIH_2O) for one hour in a heating block or hot water bath. Each sample were made up to volume with dilute HCl and then split into 15 g or 30 g digestion for Inductively Coupled Plasma Mass Spectrometry (ICP-MS) analysis in parts per million (ppm).

3. RESULTS AND DISCUSSION

3.1 Geology of the Area

The study area lies between latitude 11° 22' to 11° 30'N and longitude 07° 23' to 07° 30'E and covers a total area of 195 km^2 and falls within the north western zone of the Nigerian basement complex. The Migmatite-Gneiss Complex of the study area has heterogenous assemblages of migmatites, granite gneiss and augen gneiss (Fig. 1).

The migmatites occurs as low-lying outcrops and boulders that are medium-grained with bandings, and they are associated with granite gneiss. The bandings are regular in form and consists of palaeosome and neosome, with stromatic and ptygmatic structures. The Granite gneiss comprises the main body of the palaeosome which consist of medium grained gneissic fabric of feldspar, quartz and biotite distributed into darker laminae. The neosome is consists of light grey medium grained granitic constituents that were introduced into the pre-existing gneissic parent's rock. They include quartz, feldspar, and little biotite and muscovite. The migmatitic gneiss outcrops at the centre of the western portion of the area, especially around Tudun Ibate, Dan Zaki and Dan Kauye as low lying outcrops and boulders. The gneissic palaeosome is highly foliated with simple fold structure. It is marked by alternating light leucosome band that is rich in quartzo-feldspathic minerals and dark melanosome band, which is composed of mafic minerals. The bands are generally discontinuous, thin and somewhat weak. The neosomes which are marked by veins of pegmatitic constituents of quartz and feldspars form a ptygmatitic structure. They form 30% of the migmatite-gneiss rock. The pegmatite veins are common and may be concordant or cross cutting and contain mostly pinkish feldspar, quartz and mica.

The granite gneiss occurs in association with migmatites, especially in the central area of the western portion of the study area. It outcrops as more resistant low-lying rock bodies and boulders along the north-western and south-western portion of the study area. Those along the river channels are highly weathered. The rock is medium-gained light grey to grey in colour and it is well foliated. The foliation is marked by segregation of quartz-feldspar and biotite-rich successions in a north-south direction. The ferromagnesian minerals tending to concentrate in parallel alignment of darker bands, the

coloured minerals consists of biotite and hornblende, while the light coloured bands are quartz and feldspar rich. The granite gneiss around Ungwan Balarabe in the north has green amphibole along the darker bands. The rocks are jointed with one set of jointing system trending north-south and the others trending east-west. The quartz-feldspar veins are concordant and sometimes develop pinch and swell structures. The pegmatite veins run parallel to the foliation of these rocks, some few are discordant. There are portions of the granite gneiss that has folded banding, somewhat complexly, within the migmatite, and there are areas where the granite gneiss consists of weakly foliated granite rock which gives the granite gneiss a migmatitic feature, thus called migmatitic granite gneiss. The folding gives the lecucocratic portion ptygmatitic structure. It is a light grey leucocratic rock with the banding varying in thickness and continuity. The individual bandings vary in thickness from fraction of a centimetre to several centimetres, the banding in some places are split into smaller units.

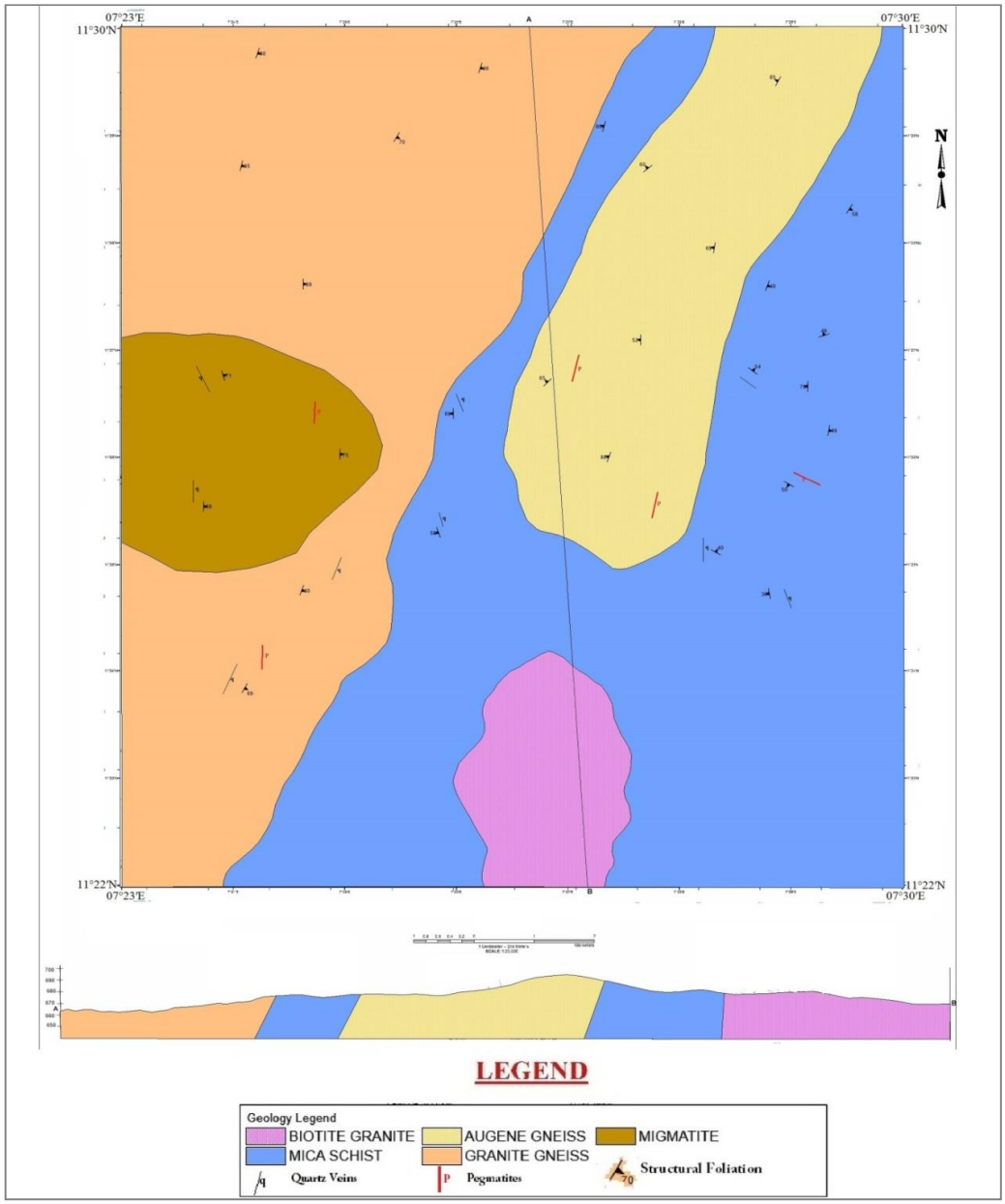

Fig. 1. Geological map and cross section of the study area

The Augen gneiss occupies about 20% of the area, and it occurs as boulders and low lying outcrops in the north-east and extends towards the centre of the study area. They are prominent around part of Rafin Gora, Ungwan Sambo, and Tandaman area as boulders and low-lying outcrops. The rock is dark grey in colour and weakly foliated, and bounded by mica schist. It is characterized by feldspathic augens enclosed in a finer grained groundmass of feldspar, quartz and ferromagnesian minerals which are weakly foliated. Generally, the shape of the feldspar porphyroblasts is irregular, the colour of the porphyroblasts is pale pink and they are embedded in a groundmass of flattened quartz crystals, chlorite and biotite. The feldspar augen has inclusion of wisps and small belbs of the groundmass, especially quartz. The grain size of the rock is finer, more foliated and less porphyroblastic in the north, while those in the central area are more porphyroblastic and less foliated. This shows that the rock experienced more shearing in the north than in the central area.

The other rocks in the study area include the biotite granite and mica schist. This granitic rock is located in the southern part of the study area; it occurs as grey coloured boulders. They are massively fractured plutons with irregular shapes that intruded the schist belt. The mica schists are generally soft, weathered and poorly exposed; most exposures occur mostly along river channels and road cuttings. They are extensive and constitute about 40% of the entire study area; they are in contact with migmatite-gneiss, augen gneiss, and biotite granite.

3.2 Geochemistry

Major and trace elements distribution of the migmatite-gneisses of the area are represented in Table 1.

Major element concentrations in the studied rocks fully reflect their felsic granitic character. The granitic composition and the igneous nature of these rocks is supported by their position in various diagrams such as Na_2O/Al_2O_3 vs K_2O/Al_2O_3 (after Garrells and Mackenzie [17]) and TiO_2 vs SiO_2 discrimination diagram (after Tarney [18], as shown in Fig. 2.

AFM plots of the all the rocks enable classification of the rocks into calk-alkaline and tholeiite series based on the proportion of their Na_2O, K_2O, Fe_2O_3, and MgO content. The migmitite-gneisses plot in the field of calc-alkaline series owing to the fact that these rocks have high percentage of Na_2O and K_2O, relative to Fe_2O_3 and MgO (Fig. 3)

It contain >2.0% high K_2O content in the range of 2.36 wt% to 6.55wt% (an average of 4.83wt%). The total alkalis A/NK [molar (Al_2O_3/Na_2O+K_2O)] and A/CNK [molar $(Al_2O_3/CaO+Na_2O+K_2O)$] contents range from 1.15–1.50 and 0.7–1.22 respectively (Table 1). The migmatite-gneisses are metaluminous to weakly peraluminous with the Alumina Saturation Index (ASI) = molar [Al/Ca+Na+K] contents which range from 0.7–1.22 which is characteristic of I-type rock (Fig. 4).

According to the classification of granitoid rocks by Frost et al. [19] using SiO_2 (wt.%) vs. Fe*-number [molar $Fe_2O_3/(Fe_2O_3 + MgO)$], most of the plots of migmatite-gniesses lie in the compositional field for Caledonian post-collisional plutons (Fig. 5a). This diagram shows that the augen gneiss belong to the magnesian group (only 1 sample of augen gneiss belong to ferroan group) while migmatite and granite gneiss belong to the ferroan group (only 1 sample of migmatite and granite gneiss belong to magnesian group).

In SiO_2 (wt.%) vs. (Na_2O+K_2O+CaO) (wt.%) diagram (modified alkali lime index, MALI) of Frost et al. [19], with increasing SiO_2 composition, the granite gneiss and augen gneiss are of alkali-calcic and the migmatite mainly of calc-alkalic (Fig. 5b).

In the migmatite-gneiss rocks, Al_2O_3, CaO, MgO, TiO_2, Fe_2O_3, P_2O_5, Ba and Sr display a linear negative correlation with SiO_2 in the Harker plot suggesting fractional crystallization. The variations of Na_2O correlate positively with SiO_2 up to 70% SiO_2 and then correlate negatively, K_2O is broadly positively correlated with SiO_2 (Fig. 6).

In the incompatible trace-element concentrations normalized by Chondrite, after Thompson [20] (Fig. 7a), the migmatite-gneisses display a near negative linear trend characterised by decreasing abundance from large ion lithophile elements (LILE) down to high field strength elements (HFSE).

The migmatite display gentle slope with positive Rb, U, Th, Ta, K, Pb, Sr, Nd, Zr, Sm, Hf, La, Dy, with slightly Cs, Th, enrichment, there are depletion in Ba, Ce, Pr, P, Ti, Nb. The granite gneiss show enrichment in Rb, Th, U, Pb, K, Pr, Sr, Nd, La, Sm, Dy and negative Ba, Nb, Ta, Ce, P, Zr, Ti, Cs anomaly.

Table 1. Major and trace elements composition of Migmatite, Granite gneiss, and Augen gneiss

Rock name	Migmatite	Migmatite	Migmatite	Migmatite	Migmatite	Migmatite	Granite gneiss	Granite gneiss	Granite gneiss	Granite gneiss	Granite gneiss	Granite gneiss	Granite gneiss	Granite gneiss	Augen gneiss	Augen gneiss	Augen gneiss	Augen gneiss	Augen gneiss	Augen gneiss
Sample	**ALA 28**	**ALA 28 B**	**ALA 29**	**ALA 29 B**	**ALA 30**	**ALA 31**	**ALA 14**	**ALA 15**	**ALA 15 b**	**ALA 17**	**ALA 26**	**ALA 27**	**ALA 32**	**ALA 33**	**ALA 1**	**ALA 2**	**ALA 4**	**ALA 6**	**ALA 18**	**ALA 21**
Major oxides wt%																				
SiO_2	74.01	74.09	73.64	73.95	73.71	73.9	66.27	71.78	73.72	73.37	74.09	73.68	71.34	72.46	64.68	69.94	67.74	70.51	74.15	69.94
Al_2O_3	13.45	14.52	13.69	14.73	14.73	14.01	14.6	15.26	14.5	13.63	13.87	13.74	16.02	14.82	16.41	14.73	15.23	14.67	13.76	14.6
Fe_2O_3	1.45	0.87	1.55	1.17	1.15	0.95	2.54	0.82	0.46	2	1.2	1.7	1.15	1.03	3.57	3.04	3.74	2.9	1.44	3.51
CaO	0.75	1.36	1.16	1.6	1.88	0.9	5.74	1.27	0.66	0.9	0.66	1.01	1.4	0.84	2.63	1.72	1.83	1.18	0.58	1.58
MgO	0.09	0.11	0.26	0.17	0.26	0.14	1.1	0.13	0.01	0.28	0.18	0.11	0.17	0.13	1.47	0.95	1.16	0.66	0.14	0.94
Na_2O	2.79	4.18	3.36	4.62	4.6	3.5	3.52	3.94	3	2.98	3.17	3.34	4.24	3.16	4.36	3.77	3.42	3.54	2.92	3.52
K_2O	6.44	3.75	5.02	2.83	2.36	5.26	4.31	5.43	6.55	5.56	6.34	5.44	4.1	5.84	4.4	4.4	4.19	4.65	5.03	4.76
MnO	0.06	0.01	0.02	0.02	0.02	0.01	0.12	0.02	<0.01	0.04	0.02	0.05	0.02	0.02	0.05	0.04	0.05	0.04	<0.01	0.06
TiO_2	0.08	0.09	0.17	0.12	0.12	0.09	0.3	0.07	0.02	0.17	0.12	0.1	0.1	0.07	0.61	0.47	0.66	0.38	0.09	0.49
P_2O_5	0.03	<0.01	0.05	0.02	0.04	0.02	1.11	0.02	0.02	0.05	0.02	0.02	0.04	0.01	0.29	0.14	0.17	0.1	0.01	0.14
Cr_2O_3	0.052	0.05	0.052	0.055	0.043	0.037	0.04	0.068	0.052	0.027	0.033	0.066	0.047	0.061	0.043	0.057	0.039	0.069	0.038	0.052
A/CNK	1.04	1.08	1.05	1.08	1.09	1.07	0.7	1.04	1.1	1.08	1.05	1.04	1.15	1.14	0.98	1.04	1.13	1.13	1.22	1.06
A/NK	1.16	1.33	1.25	1.38	1.45	1.22	1.4	1.24	1.21	1.25	1.15	1.21	1.4	1.27	1.37	1.34	1.5	1.35	1.34	1.33
Trace element (ppm)																				
Ba	382	719	576	533	295	684	808	1477	1201	607	541	331	406	580	1786	535	637	549	267	660
Be	3	2	1	<1	<1	<1	3	<1	<1	<1	<1	3	6	4	6	4	4	8	3	2
Co	2.9	3.3	3.2	3.5	3.7	2.7	4.5	3.6	2.6	2.7	2	3.1	3.5	3.4	8.2	8.6	8.9	7.1	3	8.3
Cs	1.9	4.4	3.1	5.4	4.8	2.3	1.7	2.1	4	2	1.3	3	3.5	3.5	4.2	10	19.1	26.8	3.4	12.5
Ga	20	13.1	12.7	15.1	15	14.4	21.9	13.2	12.7	16.1	19.3	20.5	18.9	16.2	25	21.6	23.3	20.4	17.7	19.5
Hf	3	1.8	4.3	0.9	3.1	2.6	7.8	0.3	1.1	5.8	3.6	3.1	3.3	3.4	5.9	5.9	7.1	4.3	4.1	5.8
Nb	17.3	2.8	8.2	6.5	6.7	5.7	11.5	1.5	0.5	18.9	6.4	19	7.2	5.4	14.1	14	15.8	15.3	31.2	14.5
Rb	202.5	88.5	130.1	77.6	76.7	124.9	121.8	103.1	136.7	148.6	196.7	178	145.3	191	132.4	199.7	209.7	224.9	246	217.5
Sn	2	2	2	3	3	1	7	1	1	1	1	2	2	2	3	4	6	6	3	4
Sr	67.1	188.2	138.9	200.3	201.9	172.7	471.3	440.7	337.4	154.8	130.4	63.3	94.7	97.3	874.9	237.1	257.3	193.6	56.3	223
Ta	0.3	0.6	0.6	1.7	0.7	0.3	0.7	<0.1	<0.1	0.6	0.2	0.5	0.4	0.4	1.1	1.1	1.7	2.6	1.4	2.1
Th	26.5	1.9	18.6	6.2	4.6	19.1	42.6	8.3	11.2	59.7	18.5	23.6	12.5	7.3	12.3	27.5	24.8	29.7	39.7	27.8
U	10.4	0.8	1.5	2.3	1.3	1.6	6.8	0.7	1	5.2	4.3	9.9	1.3	0.9	2.4	7.7	8.2	8.9	8.3	12.6
V	<8	<8	<8	<8	<8	<8	19	<8	<8	<8	<8	<8	<8	<8	66	48	57	33	<8	33
Zr	91	65.9	133.4	27.6	109.6	71.8	293.4	12.3	31.9	173.4	105.8	91.2	102.3	96.8	237.1	221.4	275.1	161.7	116.2	207.2

Rock name	Migmatite	Migmatite	Migmatite	Migmatite	Migmatite	Migmatite	Granite gneiss	Granite gneiss	Granite gneiss	Granite gneiss	Granite gneiss	Granite gneiss	Granite gneiss	Granite gneiss	Augen gneiss	Augen gneiss	Augen gneiss	Augen gneiss	Augen gneiss	Augen gneiss
Sample	**ALA 28**	**ALA 28 B**	**ALA 29**	**ALA 29 B**	**ALA 30**	**ALA 31**	**ALA 14**	**ALA 15**	**ALA 15 b**	**ALA 17**	**ALA 26**	**ALA 27**	**ALA 32**	**ALA 33**	**ALA 1**	**ALA 2**	**ALA 4**	**ALA 6**	**ALA 18**	**ALA 21**
Y	77.4	3.7	14.6	11.1	6.9	3.9	17.5	3.1	2.9	19.9	4.9	77.3	13.3	6.1	11.5	14.9	14.8	22.4	41.5	19
La	33.7	5	37.5	3.6	8.7	30.3	101	23.5	13.5	106.7	27.3	29.9	67.9	26.5	39.8	53.2	20.7	44.3	44.6	51
Ce	59.9	8.3	65.7	2.5	17.3	56.2	205.1	41.2	27.8	187.1	48	53.6	68.3	33.8	86.4	85	82.4	73.2	67.1	95.4
Pr	5.9	1.02	6.99	0.48	1.72	5.65	23.79	4.21	2.73	20.35	5.1	5.22	15.41	6.05	9.44	9.88	6.01	9.31	8.65	10.01
Nd	17.7	3.5	23.3	1.9	6.6	18.5	86	15.3	9.6	69.7	17.9	17.7	49.5	20.5	36.5	33.2	22.6	33.5	30.3	36.2
Sm	3.97	0.69	4.99	0.55	1.43	3.4	11.1	2.08	1.65	12.1	3.25	3.8	8.65	3.51	6.6	5.34	4.83	6.17	6.15	5.96
Eu	0.52	0.7	0.7	0.77	0.71	0.78	2.15	0.75	0.51	0.87	0.59	0.48	1.1	0.79	1.48	0.94	0.81	1.05	0.72	1.06
Gd	5.17	0.68	4.1	0.93	1.43	2.84	6.83	1.51	1.14	9.95	2.26	4.95	6.08	2.57	4.77	4.42	3.66	5.19	5.9	4.87
Tb	1.22	0.12	0.53	0.2	0.24	0.31	0.68	0.17	0.14	1.18	0.29	1.22	0.84	0.35	0.54	0.58	0.52	0.7	1.06	0.62
Dy	9.04	0.75	2.77	1.56	1.2	1.19	3.1	0.79	0.58	5.26	1.21	9.39	3.44	1.54	2.4	2.69	2.83	4.03	6.46	3.29
Ho	2.53	0.11	0.43	0.38	0.27	0.16	0.6	0.11	0.08	0.73	0.22	2.48	0.56	0.24	0.39	0.5	0.5	0.71	1.28	0.61
Er	8.67	0.34	1.18	1.11	0.66	0.24	1.48	0.17	0.23	1.6	0.48	8.42	1.15	0.6	0.97	1.23	1.41	1.79	4.19	1.76
Tm	1.47	0.05	0.15	0.17	0.1	0.03	0.22	0.03	0.04	0.23	0.06	1.41	0.15	0.07	0.13	0.21	0.2	0.3	0.62	0.27
Yb	9.85	0.43	0.92	1.33	0.75	0.21	1.45	0.16	0.29	1.17	0.33	9.09	0.78	0.46	0.87	1.29	1.44	1.85	4.1	1.49
Lu	1.34	0.06	0.16	0.19	0.11	0.03	0.18	0.01	0.03	0.18	0.05	1.37	0.11	0.08	0.12	0.17	0.22	0.28	0.59	0.22
SumREE	160.98	21.75	149.42	15.67	41.22	119.84	443.68	89.99	58.32	417.12	107.04	149.03	223.97	97.06	190.41	198.65	148.13	182.38	181.72	212.76
Mo	4.5	2.3	2.4	2.8	2.4	2.7	2.3	3.1	2.8	1.7	1.9	4.8	3.7	3.6	2.2	3.9	1.2	3.5	2.7	4.4
Cu	25.1	7.4	7.1	8.1	7.8	5.9	6.2	10.8	8.5	4.7	6.7	12.2	10.7	12.6	31.1	15.6	19.7	14.6	7.3	21.5
Pb	12.7	6.2	4.3	8.4	8	7.6	11	11.9	8.9	6.4	6.9	12	9.8	9.8	5.9	7.7	8.5	13.7	14.6	9.2
Zn	22	12	27	17	21	14	14	13	4	31	22	23	14	15	70	56	61	40	18	57
Ni	104.5	86.6	68.9	96.3	91.8	77	70.5	110.1	102.7	60.2	50.2	117.3	108.4	103.8	77	98.9	59.8	125.2	78.4	99.3
Tl	0.2	0.1	0.3	0.2	0.2	0.1	<0.1	<0.1	<0.1	0.4	0.3	0.3	0.2	0.2	0.5	0.8	0.9	0.6	0.3	0.7
LaN	108.71	16.13	120.97	11.61	28.06	97.74	325.81	75.81	43.55	344.19	88.06	96.45	219.03	85.48	128.39	171.61	66.77	142.9	143.87	164.52
CeN	74.13	10.27	81.31	3.09	21.41	69.55	253.84	50.99	34.41	231.56	59.41	66.34	84.53	41.83	106.93	105.2	101.98	90.59	83.04	118.07
PrN	48.36	8.36	57.3	3.93	14.1	46.31	195	34.51	22.38	166.8	41.8	42.79	126.31	49.59	77.38	80.98	49.26	76.31	70.9	82.05
NdN	29.5	5.83	38.83	3.17	11	30.83	143.33	25.5	16	116.17	29.83	29.5	82.5	34.17	60.83	55.33	37.67	55.83	50.5	60.33
SmN	20.36	3.54	25.59	2.82	7.33	17.44	56.92	10.67	8.46	62.05	16.67	19.49	44.36	18	33.85	27.38	24.77	31.64	31.54	30.56
EuN	7.07	9.52	9.52	10.48	9.66	10.61	29.25	10.2	6.94	11.84	8.03	6.53	14.97	10.75	20.14	12.79	11.02	14.29	9.8	14.42
GdN	19.96	2.63	15.83	3.59	5.52	10.97	26.37	5.83	4.4	38.42	8.73	19.11	23.47	9.92	18.42	17.07	14.13	20.04	22.78	18.8
TbN	25.74	2.53	11.18	4.22	5.06	6.54	14.35	3.59	2.95	24.89	6.12	25.74	17.72	7.38	11.39	12.24	10.97	14.77	22.36	13.08
DyN	28.07	2.33	8.6	4.84	3.73	3.7	9.63	2.45	1.8	16.34	3.76	29.16	10.68	4.78	7.45	8.35	8.79	12.52	20.06	10.22
HoN	35.24	1.53	5.99	5.29	3.76	2.23	8.36	1.53	1.11	10.17	3.06	34.54	7.8	3.34	5.43	6.96	6.96	9.89	17.83	8.5

Rock name	Migmatite	Migmatite	Migmatite	Migmatite	Migmatite	Migmatite	Granite gneiss	Granite gneiss	Granite gneiss	Granite gneiss	Granite gneiss	Granite gneiss	Granite gneiss	Granite gneiss	Augen gneiss	Augen gneiss	Augen gneiss	Augen gneiss	Augen gneiss	Augen gneiss
Sample	**ALA 28**	**ALA 28 B**	**ALA 29**	**ALA 29 B**	**ALA 30**	**ALA 31**	**ALA 14**	**ALA 15**	**ALA 15 b**	**ALA 17**	**ALA 26**	**ALA 27**	**ALA 32**	**ALA 33**	**ALA 1**	**ALA 2**	**ALA 4**	**ALA 6**	**ALA 18**	**ALA 21**
ErN	41.29	1.62	5.62	5.29	3.14	1.14	7.05	0.81	1.1	7.62	2.29	40.1	5.48	2.86	4.62	5.86	6.71	8.52	19.95	8.38
TmN	45.37	1.54	4.63	5.25	3.09	0.93	6.79	0.93	1.23	7.1	1.85	43.52	4.63	2.16	4.01	6.48	6.17	9.26	19.14	8.33
YbN	47.13	2.06	4.4	6.36	3.59	1	6.94	0.77	1.39	5.6	1.58	43.49	3.73	2.2	4.16	6.17	6.89	8.85	19.62	7.13
LuN	41.61	1.86	4.97	5.9	3.42	0.93	5.59	0.31	0.93	5.59	1.55	42.55	3.42	2.48	3.73	5.28	6.83	8.7	18.32	6.83
Eu/Eu*	0.35	3.12	0.47	3.29	1.52	0.77	0.75	1.29	1.14	0.24	0.67	0.34	0.46	0.8	0.81	0.59	0.59	0.57	0.37	0.6
LaN/YbN	2.31	7.84	27.48	1.82	7.82	97.28	46.96	99.02	31.38	61.48	55.77	2.22	58.69	38.84	30.84	27.8	9.69	16.14	7.33	23.08
LaN/SmN	5.34	4.56	4.73	4.12	3.83	5.61	5.72	7.11	5.15	5.55	5.28	4.95	4.94	4.75	3.79	6.27	2.7	4.52	4.56	5.38
CeN/YbN	1.57	4.99	18.47	0.49	5.97	69.22	36.59	66.61	24.8	41.36	37.62	1.53	22.65	19.01	25.69	17.04	14.8	10.23	4.23	16.56
CeN/SmN	3.64	2.9	3.18	1.1	2.92	3.99	4.46	4.78	4.07	3.73	3.56	3.4	1.91	2.32	3.16	3.84	4.12	2.86	2.63	3.86
EuN/YbN	0.15	4.63	2.16	1.65	2.69	10.56	4.22	13.33	5	2.11	5.08	0.15	4.01	4.88	4.84	2.07	1.6	1.61	0.5	2.02
Rb/Sr	3.02	0.47	0.94	0.39	0.38	0.72	0.26	0.23	0.4	0.96	1.51	2.81	1.53	1.96	0.15	0.84	0.81	1.16	4.37	0.97
U/Pb	0.11	0.01	0.04	0.02	0.01	0.004	0.016	0.0008	0.003	0.028	0.007	0.11	0.011	0.0081	0.02	0.02	0.026	0.02	0.04	0.024
Lu/Hf	0.45	0.03	0.04	0.21	0.03	0.01	0.02	0.03	0.03	0.03	0.01	0.44	0.03	0.02	0.02	0.03	0.03	0.06	0.14	0.04
Sm/Nd	0.22	0.2	0.21	0.29	0.22	0.18	0.13	0.14	0.17	0.17	0.18	0.21	0.17	0.17	0.18	0.16	0.21	0.18	0.2	0.16
Th/U	2.55	2.37	12.4	2.7	3.54	11.94	6.27	11.86	11.2	11.48	4.3	2.38	9.62	8.11	5.13	3.57	3.02	3.34	4.78	2.21
Th/Yb	2.69	4.42	20.22	4.66	6.13	90.95	29.38	51.87	38.62	51.03	56.06	2.6	16.03	15.87	14.14	21.32	17.22	16.05	9.68	18.66
Ta/Yb	0.03	1.39	0.65	1.28	0.93	1.43	0.48	0.62	0.35	0.51	0.61	0.06	0.51	0.87	1.26	0.85	1.18	1.41	0.34	1.41
Ce/Pb	4.72	1.34	15.28	0.3	2.16	7.4	18.64	3.46	3.12	29.23	6.96	4.47	6.97	3.45	14.64	11.04	9.69	5.34	4.6	10.37
Ba/Nb	22.08	256.79	70.24	82	44.03	120	70.26	984.67	2402	32.12	84.53	17.42	56.39	107.41	126.67	38.21	40.32	35.88	8.56	45.52
Sr/Y	0.87	50.87	9.51	18.04	29.26	44.28	26.93	142.16	116.35	7.78	26.61	0.82	7.12	15.95	76.08	15.91	17.38	8.64	1.36	11.74

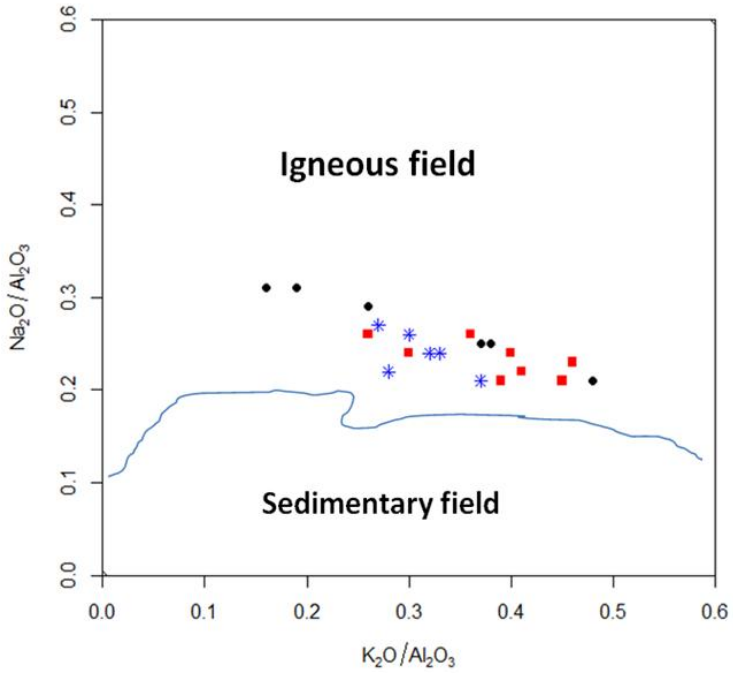

(a)

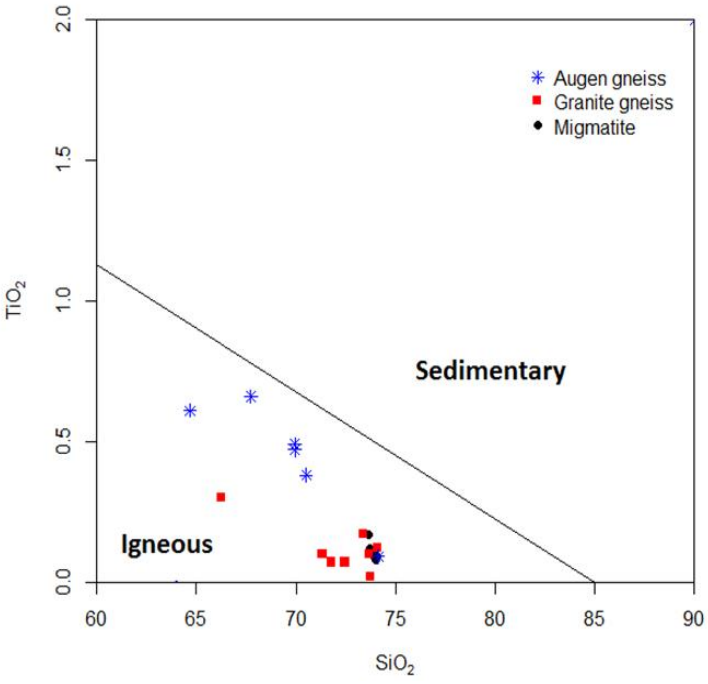

(b)

Fig. 2. (a) Na_2O/Al_2O_3 versus K_2O/Al_2O_3 plot (after Garrells and Mackenzie, 1971); and (b) TiO_2 versus SiO_2 discrimination diagram (after Tarney, 1977) showing the protolith of migmatite-gneisses in the study area

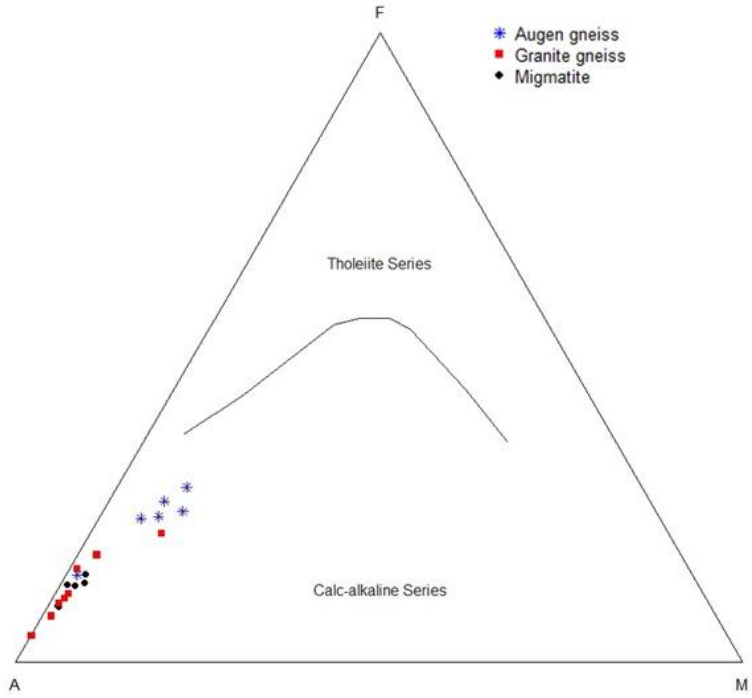

Fig. 3. AFM diagram (Irvine and Baragar, 1971), where A = Na_2O+K_2O, F = Fe_2O_3, M = MgO

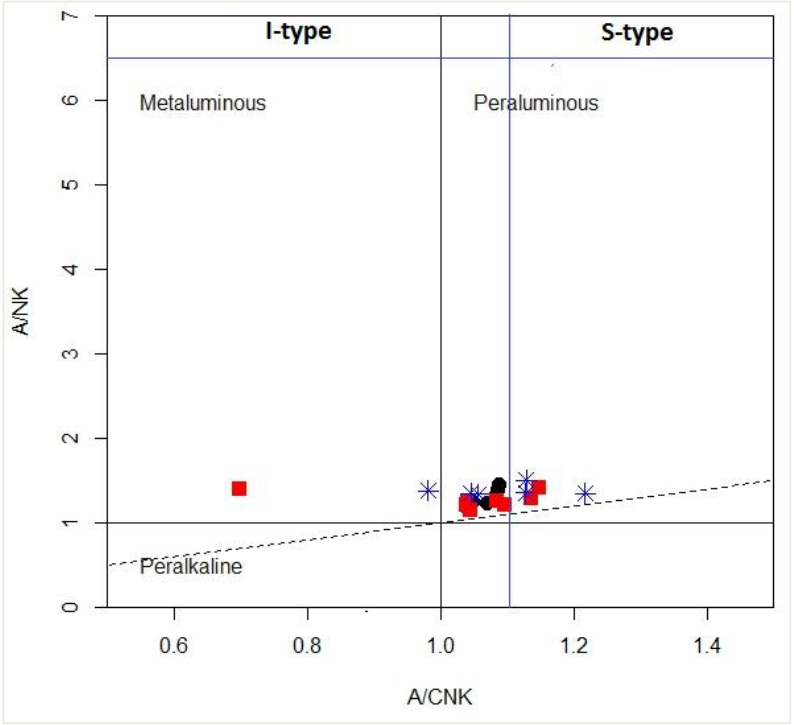

Fig. 4. Geochemical plot of A/CNK versus A/NK of migmatite-gneisses showing the distribution of the rocks from metaluminous to weakly peraluminous field (after Shand, 1943)

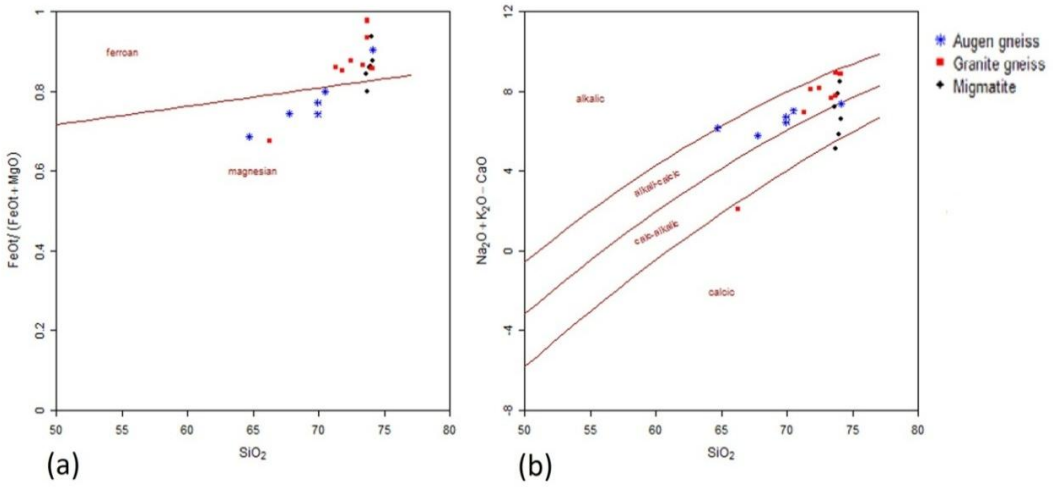

Fig. 5. Binary plots of the migmatite-gneisses (after Frost et al. 2001) (a) SiO_2 versus $Fe_2O_3/(Fe_2O_3+MgO)$ (b) SiO_2 versus (Na_2O+K_2O-CaO)

Augen gneiss is characterised by negative Ba, Nb, Ce, Ti, Ta, Sr, P and enriched in Cs, Rb, Th, U, Pb, Pr, Nd, La, Zr, Sm, Dy.

The characteristics of the trace elements is a reflection of the various sources of the derived protolith of migmatite-gneisses, with Nb, Ta, and Ti depletion along with the enrichment in K and Pb indicating arc rocks or continental crustal signatures. High oxygen (O_2) fugacity is required to allow HFSE fractionation which produces Eu anomaly [21], with negative Eu anomaly more probable to occur [22].

The ratios of incompatible trace elements such as Th/U (2.21–12.4), Th/Yb (2.60–90.95), Ta/Yb (0.03-1.43), Ce/Pb (mainly 0.30–29.23) and high Ba/Nb (8.56–2402), are comparable to those of continental crust [23,24], and those at active continental margins [25].

The Eu anomalies could be accredited to the different contents of plagioclase which is characteristic of processes recorded in pluton magma chambers. Generally, Eu anomalies are negative (Eu/Eu* = 0.24–0.81, an average of 0.56), samples ALA 33 and ALA 15B have small or negligible Eu anomalies (Eu/Eu* = 0.81 and 1.14, respectively), except for samples ALA 15, ALA 30, ALA 28B and ALA 29B, which have positive Eu anomalies (Eu/Eu* = 1.29, 1.52, 3.12 and 3.29, respectively). A negative Eu anomaly in almost all the analyzed samples, indicate that the migmatite-gneisses are highly fractionated, except for four samples that show positive Eu anomaly and no anomaly observed in two. This contrasting Eu behaviour can be attributed to the difference in the geodynamic setting (tectono-metamorphic and tectono-magmatic) of the emplacement of these rocks. With the exception of samples ALA15 and ALA15B that shows high value of Sr/Y (142.16 and 116.35 respectively), the values of Sr/Y are less than 100 (<100) which indicate that the rocks are subduction-related, thus, crustal-derived or subduction-modified component in mantle source is evident. Geochemical differences are apparent with regards to Sr/Y ratios in relation to Y; part of the granite gneisses (samples ALA15 and ALA15B) and migmatites (samples ALA28B and ALA31) tend to have elevated Sr/Y ratios at low Y contents, which is a feature observed in subduction-related activities where young and hot slabs are being subducted leading to differences in subduction geochemical fluxes.

The results of the abundance and distribution of the rare earth elements (REE) in the migmatite-gneisses of the study area are presented in Table 1. The results show that the migmatite-gneisses are highly enriched in the lighter rare earth elements (LREE) Sm, Pr, Nd, La and Ce, in that order of increasing abundance, with average values of 4.81 ppm, 7.90 ppm, 27.50 ppm, 38.44 ppm, 68.22ppm, respectively; and relatively depleted in the heavy rare earth elements (HREE) Lu, Tm, Tb, Ho, Yb and Er, with average values ranging 0.28 ppm, 0.30 ppm, 0.58 ppm, 0.65ppm, 1.91 ppm and 1.88 ppm respectively (Table 1).

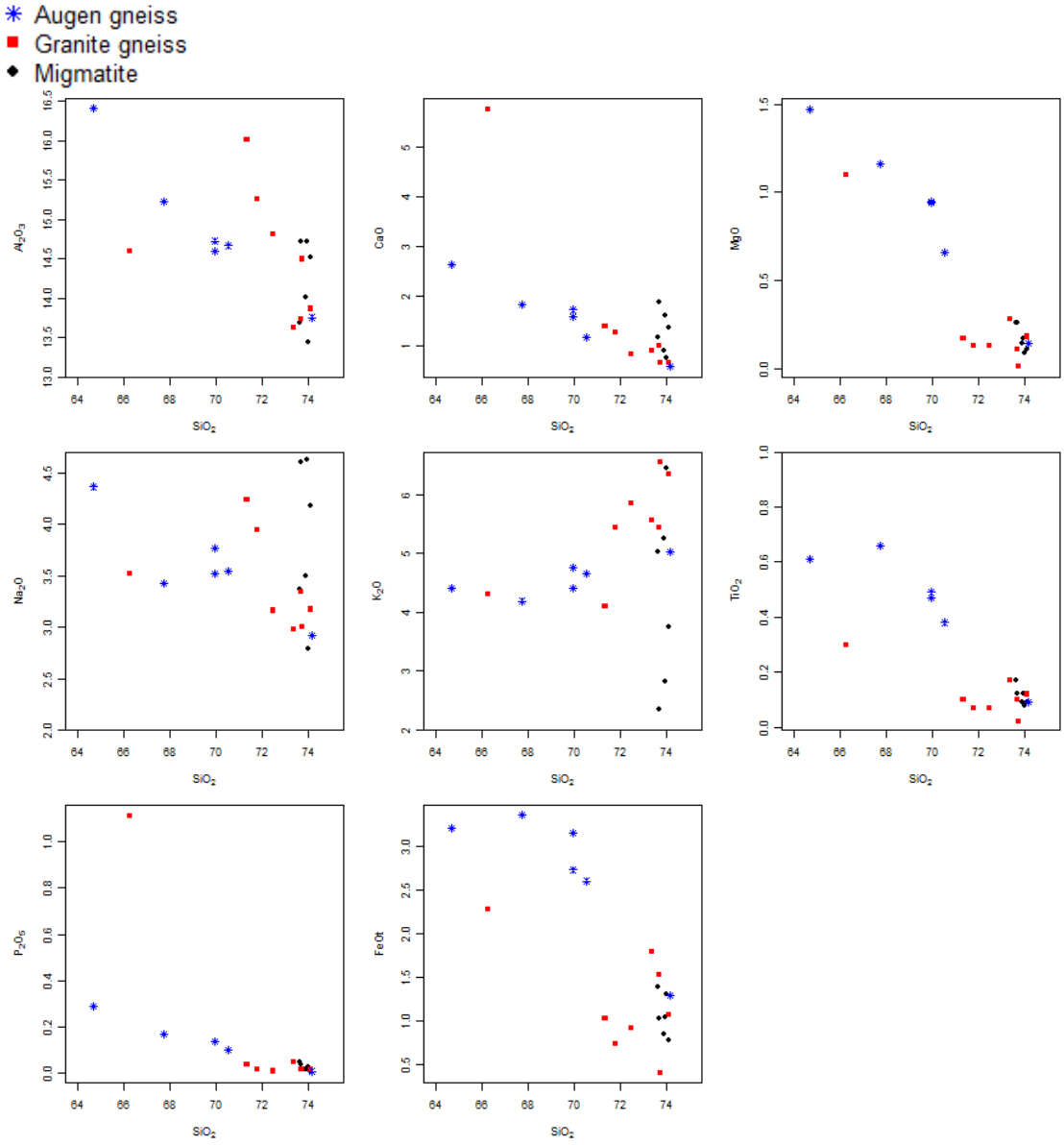

Fig. 6. Harker diagrams of major elements for the migmatite-gneisses

The total rare earth elements abundance {TREE = Σ(La + Ce + . . . + Lu)} varies from 508.88ppm in the migmatite, to 1586.21 ppm in the granite gneiss, through 1114.05 ppm in the augen gneiss.

The REE patterns (Fig. 7b) are highly fractionated, La/Yb = 1.8–97.92, average of 32.33), showing a relatively sharp decrease from La to Sm (chondrite-normalized La/Sm = 2.7–7.11, average of 4.94) and a flat heavy REE (HREE) profile (chondrite-normalized Tb/Yb = 0.55–6.54, average of 2.49).

3.3 Discussion

3.3.1 Classification

The migmaitie-gneisses can be classified according to the presumed origin of the parent rocks. The rocks plot in the igneous field which indicates an igneous protolith (Fig. 2). On the classification scheme of Frost et al. [19] in Fig. 5, the migmatite-gneisses display magnesian to ferroan characteristics, and alkali-calcic to calc-alkali characteristics. They are metaluminous to weakly peraluminous, and I-

type in nature, with S-type characteristics in some augen gneiss samples (ALA17, ALA18, and ALA19) and granite gneiss samples (ALA13, and ALA14).

Results indicate that the rocks are I-type, metaluminous to weakly peraluminous [ASI= molar Al/(Ca + Na + K] contents which range from 0.7–1.22, and having wide range of silica contents are product of the partial melting of mafic to felsic meta-igneous source, possibly by partial melting of tonalitic to granodioritic crustal rocks at low pressure, with some S-type character [26].

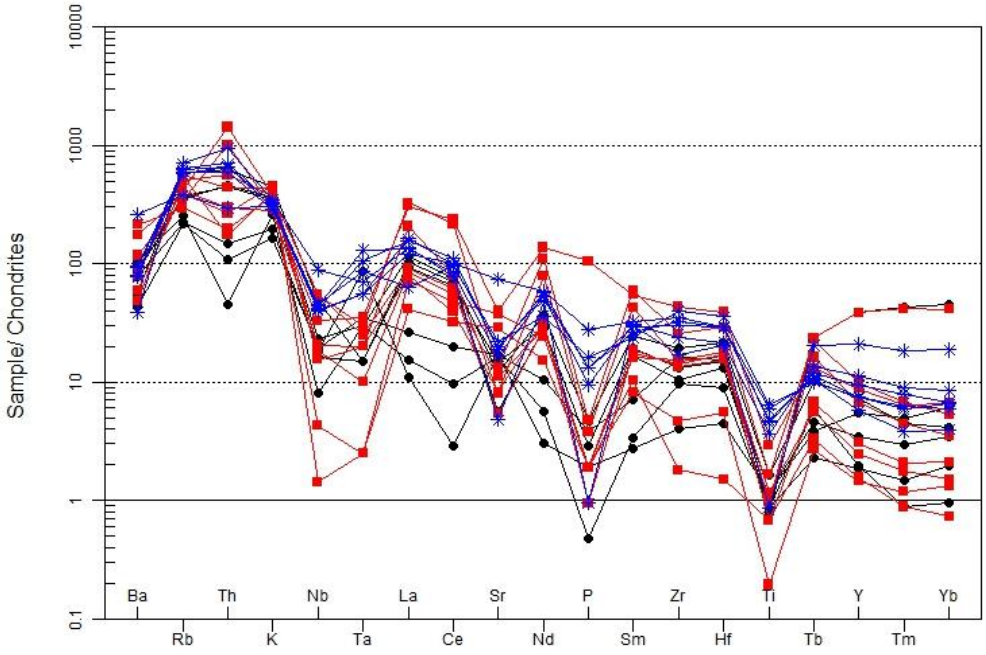

(a)

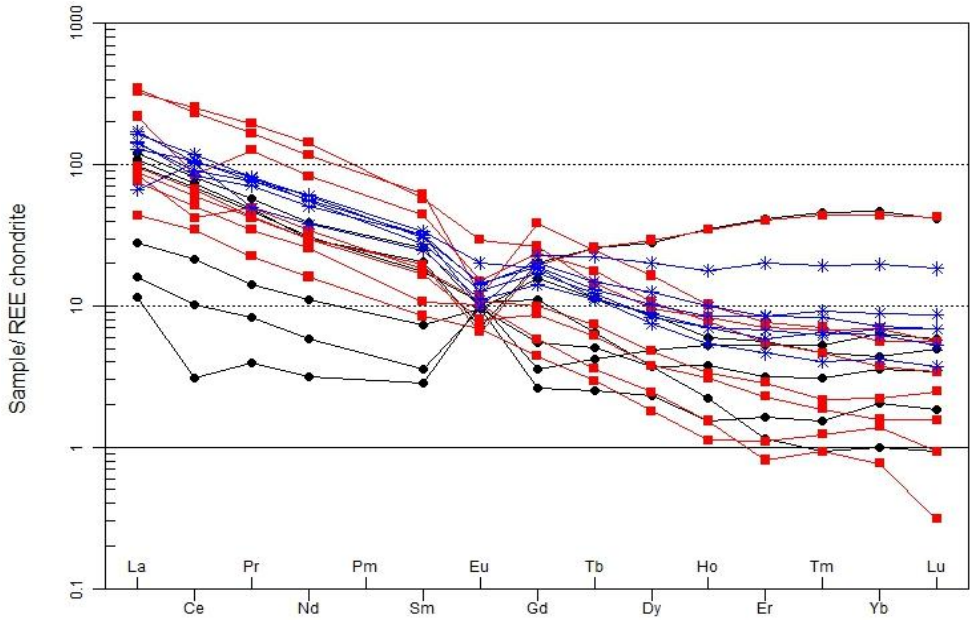

(b)

Fig. 7. (a) Chondrite-normalized incompatible element patterns for mimatite-gneisses. Normalization values from Thompson (1982), and (b) Chondrite-normalized REE abundances for migmatite-gneisses. Normalization values fromBoynton (1984)

These characteristics together with the positions of the samples on the Na_2O/Al_2O_3 versus K_2O/Al_2O_3 discrimination diagram (after Garrels and Mackenzie [17]), and TiO_2 versus SiO_2 plot (after Tarney [18]) further support I-type affinity for the migmatite-gneisses.

3.3.2 Petrogenesis

A study into the origin of the migmatite-gneisses in the study area indicates an evolutionary trend in the major element values. The Al_2O_3, Na_2O, CaO, MgO, TiO_2, Fe_2O_3, MgO, TiO_2 and P_2O_5 decrease, with relatively little scatter, with increasing SiO_2 and, although with great scatter, negative correlations are also seen between SiO_2 and Al_2O_3, and Na_2O, Zr and Y. These observations suggest, on one side, closed system behaviour during metamorphism, and, on the other side, a comagmatic origin of the igneous protolith (with the possible exception of the two most silica-rich samples).

Fractional crystallization which encompasses the formation of plagioclase and biotite as indicated by the negative correlation between the values of SiO_2 versus CaO, MgO, Fe_2O_3, are in congruent with the field and petrographic proof of plagioclase and biotite abundance. The melting of the protolith occurred under hydrous conditions as indicated by the presence of hydrous minerals like biotite. The migmatite-gneisses of the study area are product of reworking of the rocks during the Pan-African as seen in the high Na_2O and K_2O values, along with mainly alkali-calcic affinity, which can be compared to those of Archaean migmatite-gneisses.

The relatively low Sr/Y (<100) ratio and Y contents characterize transitional compositions between Archean and an arc rocks [1], which allows us to suggest evolution of the composition of the primary melt as a result of assimilation of Archean crust material or mixing of the basic melt with acid melt formed during crust melting.

On the Sr/Y vs Y diagram (Fig. 8a), the rock suites are projected into the melts that are typical of arc rocks and Adakite [27]. Some samples of the granite gneisses (samples ALA15 and ALA15B) and migmatites (samples ALA28B and ALA31) tend to show elevated Sr/Y ratios at low Y contents, features typical of Adakite. The contents of Y in the rocks are generally higher relative to Sr/Y ratio, features typical of basalt-andesite-dacite-rhyolite (BADR). The trend in Sr/Y ratio relative to Y contents in the rocks reflects the different components and processes of crystal fractionation, crustal melting and/or contamination that operated during magma ascent, thus, reflecting two distinct sources of the felsic protolith namely crustal melts and slab melts [28].

The geochemical signature of the migmatite-gneisses is characterized by the enrichment of K, Rb, Ba, which are LILE and negative Nb and Ta, which are similar to those of Archean rocks, thus, probably formed by melting of basalt in a subduction setting [29]. Fractional crystallization is reflected in the differences in the samples which indicate melts formed by mixing of mafic melt with crustal components during ascent, and thus, the migmatitie-gneisses follow sub-parallel alkali-lime trends during differentiation [19]. The migmatite-gneisses generally belong to magnesian to ferroan, and alkali-calcic to calc-alkali (Figs. 5a and 5b), metaluminous to weakly peraluminous (Fig. 4). The augen gneisses are more magnesian while the granite gneisses and migmatites are more ferroan, which implies that the source of the augen gneiss protolith is from a more oxidized source compared to a more reduced source of granite gneiss and migmtite protolith; thus, the occurrence of extensive fractionation from magnesian towards iron-rich alkali compositions.

The Fe-number (Fe*) is effective in separating granitoids into magnesian and ferroan, as the value of the indices gives information about the history of differentiation of the magma, particularly with high SiO_2 content between 50 wt% to 75 wt% which is a reflection of the rocks. The origin of the migmatite-gneisses is thus from metaigneous source rocks, as evident in the geochemical signature of metaluminous to weak peraluminous, proportionately high sodic values, with broad silica values.

The rocks have high-K affiliation with K_2O values ranging from 2.36 wt% to 6.55 wt% (an average of 4.83 wt%), which is also a reflection of the protoliths, which are more differentiated granitoids. This signifies that the migmatite-gneisses have their origin at the convergent margin setting where the process of remelting, mixing and differentiation of the crust occurred.

3.3.3 Tectonic setting

In general, the chondrite-normalized trace elements for the migmatite-gneisses are characterized by the enrichment of LREE and

LILE with depleting HREE and HFSE as illustrated in the near linear negative pattern, which is characteristic of magma mixing activity of the source rock; signatures like ferroan to magnesian, and alkali-calcic to calc-alkali characteristics are also evident. Ferroan and

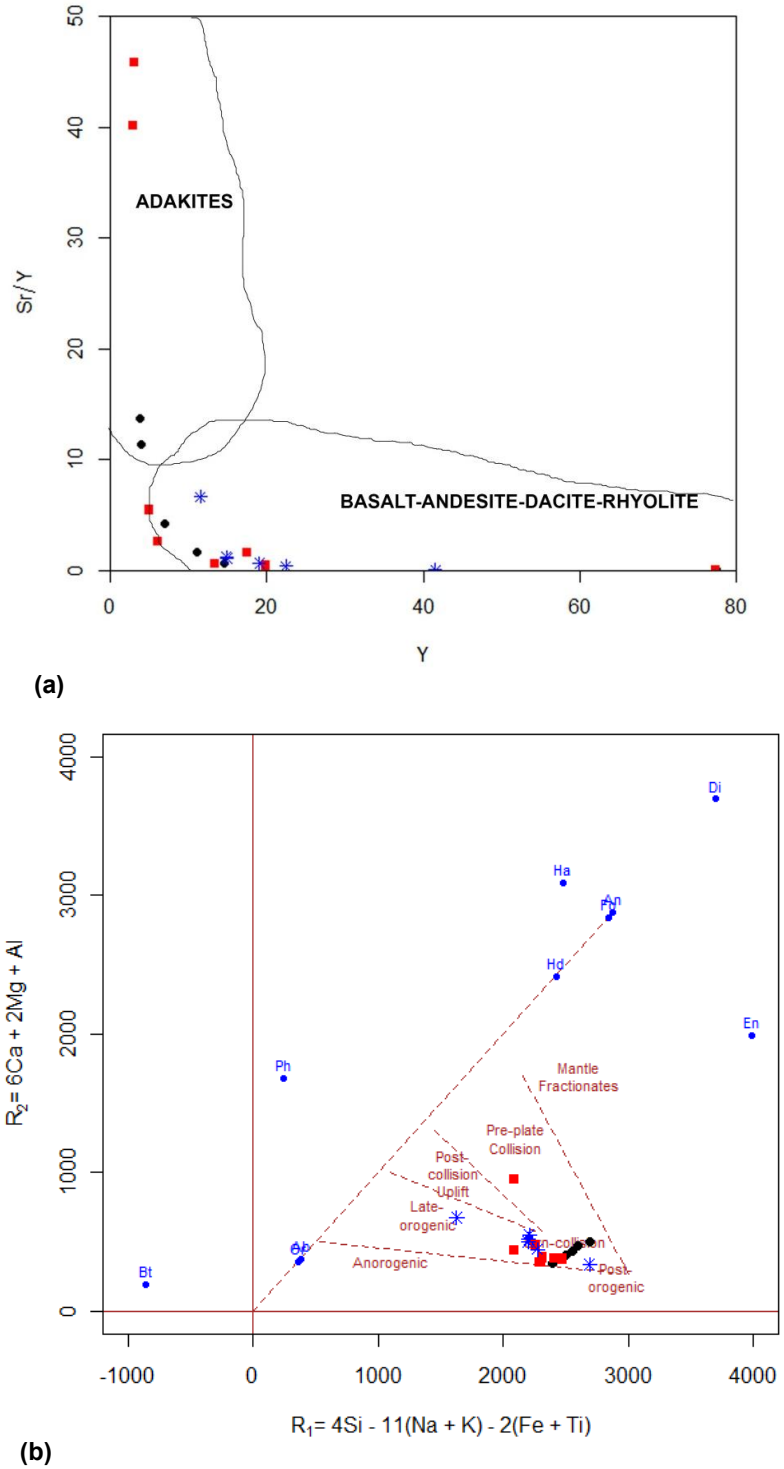

Fig. 8. Plot of (a) Sr/Y versus Y (b) R_1 versus R_2 (after, Batchelor and Bowden, 1985)

magnesian series are a reflection of the nature of the source; ferroan rocks are reflection of hydrous, reduced magmas and source region while magnesian rocks are reflection of anhydrous, oxidized magmas and source region, which are both broadly subduction-related and reflect mixing tectonic setting [19,30]. The migmatite-gneisses show a clear arc-like signature as seen in the depletion in HFSE and enrichment in LILE; and LILE enhancement relative to HFSE signifies subduction-zone enrichment and/or crustal mixing of the source region [31]. Subduction zone signatures are reflected in the enrichment of LREE with negative Eu anomalies and high-K, from arc settings and/or active continental margins settings [32].

The values of Sr/Y<100 as seen in the samples (except sample ALA15 and ALA15B with 142.16 and 116.35 respectively) and the plot of Sr/Y vs Y (Fig. 8a) are all signatures of subduction-related geotectonic setting [33].

The granitoids are product of syn-collisional igneous activities in the Late Proterozoic time as shown in the R1-R2 diagram of Batchelor and Bowden [34], thus, signifying a volcanic arc tectonic setting. In the scheme of Pearce et al. [35] and Pearce [36] (Fig. 8b), volcanic arc granite (VAG) is corresponding to syn-collisional granite, which is associated with continental arc collision that gave rise to the metaluminous to weak peraluminous I-type granitoids.

The high-K nature of the migmatite-gneisses shows the nature of the protolith; the melt have relative depletion in Nb and Ta which is typical of subduction-related magmas. The source has been modified by lithospheric subduction as it was consumed during subduction, which led to the addition of volatiles, enrichment of other incompatible elements, making it more potassic and depleted in Nb and Tb [31,37]. This is characteristic of metasomatism in relation to the Pan-African subduction.

All the analysed samples are characteristically enriched in the LREE and depleted in the HREE, the samples of whole rock REE of migmatites has a total REE abundance of 508.88 ppm, TLREE of 441.17 ppm and THREE of 67.71 ppm, yielding a TLREE/THREE ratio of 6.52 which is consistent with the general trend. The depletion maxima is recorded in the granite gneiss, which shows TREE abundance of 1586.21 ppm, TLREE (1483.64 ppm), THREE (102.57 ppm), giving a TLREE/THRE ratio of 14.47. The augen gneiss has TREE of 1114.05 ppm, TLREE (1029.81 ppm) and THREE (84.24 ppm), thus giving a TLREE/THREE ratio of 12.22. The very high enrichment trend possibly indicates high abundance of cerium earths which favours the concentration of LREE relative the HREE [38], the behaviour and range of the REE are within rocks of igneous origin.

Interpretation of the elemental abundance shows that the large ion lithophile element Rb vary from 116.72 ppm in the migmatite, through 152.65 ppm in the granite gneiss to 205.03 ppm in the augen gneiss, the rocks have an average Rb content of 157.58 ppm. The Rb content is very close to the concentration of 150 ppm for average granite, and 112 ppm for average continental crustal rock [38], thus confirming a granitic protolith for the migmatite-gneisses.

Thus, corroborating a crustal source for the protoliths of the rocks which have been affected by the Pan-African tectono-thermal events. The trend of distribution also shows the migmatite gneisses are highly differentiated and fractionated, and generally conform to the characteristics of similar rocks from other tectonic settings.

4. CONCLUSION

Precambrian migmatite-gneisses of the study area constitute the basement rocks. The high-K, calc-alkaline affinity, and negative distribution trend of Nb, Ba, and Sr as well as the enrichment of Rb and K, in the rocks suggest crustal source of the protolith derived by partial melting. In addition, the high Th/U in the rock suites suggests continental crust affinity. A slightly peraluminous nature of the rocks can indicate fractional crystallization dominated by fractionation of plagioclase as fractionation of plagioclase is expected to decrease the concentration of Al_2O_3 in the melt which will in turn decrease the aluminum saturation index, thus, the protoliths could have been derived from the partial melting of tonalitic to granodioritic crustal rocks at low pressure, thus, producing metaluminous to slightly peraluminous high-silica, ferroan, alkali-calcic to calc-alkali melts, which is why it has some S-type character. The pattern displayed is characteristic of well fractionated LREE and flat HREE, with Eu and Ba significantly negative. The trend in Sr/Y ratio relative to Y contents in the rocks reflects the different components and processes of crystal

fractionation, crustal melting and/or contamination that operated during magma ascent, thus, reflecting two distinct sources of the felsic protolith namely crustal melts and slab melts [28].

COMPETING INTERESTS

Authors have declared that no competing interests exist.

REFERENCES

1. Dada SS. Crust-forming ages and Proterozoic crustal Evoluton in Nigeria: A reappraisal of current interpretations. Precambrian Research. 1998;87(1-2):65-74.
2. Rahaman MA. Recent advances in the study of the Basement Complex of Nigeria. Precambrian Geology of Nigeria. 1988:11-41.
3. Grant NK. Geochronology of precambrian basement rocks from Ibadan, Southwestern Nigeria. Earth and Planetary Science Letters. 1970;10(1):29-38.
4. Burke KC, Freeth SJ, Grant IK. Granite gneiss in the Ibadan area, Nigeria. African Geology. Ibadan, Geology Department, University of Ibadan. 1972;103-4.
5. Onyeagocha AC. Petrology and geologic history of NW Akwanga area in Northern Nigeria. Journal of African Earth Sciences (1983). 1984;2(1):41-50.
6. Ekwere SJ, Ekwueme BN. Geochemistry of Precambrian gneisses in the eastern part of the Oban massif, Southeastern Nigeria. Geologie en Mijnbouw. 1991; 70(2):105-14.
7. Imeokparia EG, Emofurieta WO. Protoliths and petrogenesis of Precambrian gneisses from the Igbeti area, SW Nigeria. Chem. Erde. 1991;51:39-54.
8. Freeth SJ. Geochemical and related studies of West African igneous and metamorphic rocks. Unpubl. PhD. Thesis. University of Ibadan, Nigeria. 1971;240.
9. Elueze AA, Bolarinwa AT. Petrochemistry and Petrogenesis of granitic gneisses in Abeokuta area Southwestern Nigeria. Journal of Mining and Geology. 2004; 40(1):1-8.
10. Olarewaju VA. Petrology and geochemistry of the charnockitic and associated granitic rocks of Ado-Ekiti-Akure area, Southwest Nigeria. Precambrian Geology of Nigeria. Geological Survey of Nigeria. 1988;129-43.
11. Oyinloye AO. Geology, geochemistry and origin of the banded granite gneisses in the Basement complex of the Ilesha Area Southwestern Nigerian. Journal of African Earth Sciences, London. 1998;264:633-641.
12. Oyinloye AO. Geochemical Studies of granite gneisses: The implication on source determination. Journal of Chemical Society of Nigeria. 2002;26(1):131-134.
13. Oyinloye AO. Petrochemistry, pb isotope systematic and geotectonic setting of granite gneisses in Ilesha schist belt southwestern Nigeria. Global Journal of Geological Sciences. 2004;2(1):1-13.
14. Oyinloye AO. Geology and geotectonic setting of the Basement Complex rocks in Southwestern Nigeria: Implications on provenance and evolution. Earth and Environmental sciences. 2011;21(2):97-118.
15. Okonkwo CT, Ganev VY. U-Pb Geochronology of the Jebba Granitic Gneiss and its implications for the Paleoproterozoic Evolution of Jebba Area, Southwestern Nigeria. International Journal of Geosciences. 2012;3:1065-1073.
16. McCurry P. The geology of the precambrian to lower palaeozoic rocks of Northern Nigeria. A review. Geology of Nigeria. 1976;15-39.
17. Garrels RM, Mackenzie FT. Gregor's denudation of the continents. Nature. 1971;231(5302):382-3.
18. Tarney J. Petrology, mineralogy and geochemistry of the Falkland Plateau basement rocks, site 330, Deep Sea Drilling Project. Initial Reports of the Deep Sea Drilling Project. 1977;36:893-921.
19. Frost BR, Barnes CG, Collins WJ, Arculus RJ, Ellis DJ, Frost CD. A geochemical classification for granitic rocks. Journal of Petrology. 2001;42(11):2033-48.
20. Thompson RN. Magmatism of the British Tertiary volcanic province. Scottish Journal of Geology. 1982;18(1):49-107.
21. Lavecchia G, Stoppa F, Creati N. Carbonatites and kamafugites in Italy: Mantle-derived rocks that challenge subduction. Annals of Geophysics. 2006; 49(1):389-402.
22. Guo P, Niu Y, Yu X. A synthesis and new perspective on the petrogenesis of kamafugites from West Qinling, China, in a global context. Journal of Asian Earth Sciences. 2014;79:86-96.

23. Rudnick RL, Fountain DM. Nature and composition of the continental crust: A lower crustal perspective. Reviews of Geophysics. 1995;33(3):267-309.
24. Rudnick RL, Gao S. Composition of the continental crust. Treatise on geochemistry. 2003;3:659.
25. Wilson M. Igneous Petrogenesis: A global tectonic approach. Unwin Hyman, Boston. 1989;466.
26. Chappell B, White A. Two contrasting granite types. Pacific geology. 1974; 8(2):173-4.
27. Defant MJ, Drummond MS. Derivation of some modern arc magmas by melting of young subducted lithosphere. Nature. 1990;347(6294):662-5.
28. Drummond MS, Defant MJ, Kepezhinskas PK. Petrogenesis of slab-derived trondhjemite–tonalite-dacite/adakite magmas. Geological Society of America Special Papers. 1996;315:205-15.
29. Rapp RP, Watson EB, Miller CF. Partial melting of amphibolite/eclogite and the origin of Archean trondhjemites and tonalites. Precambrian Research. 1991; 51(1-4):1-25.
30. Frost BR, Lindsley DH. Occurrence of iron-titanium oxides in igneous rocks. Reviews in Mineralogy and Geochemistry. 1991; 25(1):433-68.
31. Arvin M, Rostamizadeh G. Geochemical and petrological characteristics of Deh Siahan Granitic Rocks, Southwest of Kerman, Iran: Data Bearing on Genesis. Journal of Sciences Islamic Republic of Iran. 2000;11(2):117-26.
32. Kumar GR, Sreejith C. Remelting of tonalitic crust and genesis of high-K granitoid during arc-accretion: Evidence for crustal reworking in the Kerala Khondalite Belt. Accepted for presentation in the International Symposium on Precambrian Accretionary Orogens, University of Delhi; 2011.
33. Huang XL, Niu Y, Xu YG, Yang QJ, Zhong JW. Geochemistry of TTG and TTG-like gneisses from Lushan-Taihua complex in the southern North China Craton: Implications for late Archean crustal accretion. Precambrian Research. 2010; 182(1):43-56.
34. Batchelor RA, Bowden P. Petrogenetic interpretation of granitoid rock series using multicationic parameters. Chemical Geology. 1985;48(1-4):43-55.
35. Pearce JA, Harris NB, Tindle AG. Trace element discrimination diagrams for the tectonic interpretation of granitic rocks. Journal of Petrology. 1984;25(4):956-83.
36. Pearce JA. A user's guide to basalt discrimination diagrams. Trace element geochemistry of volcanic rocks: Applications for massive sulphide exploration. Geological Association of Canada, Short Course Notes. 1996a; 12(79):113.
37. Roberts MP, Clemens JD. Origin of high-potassium, calc-alkaline, I-type granitoids. Geology. 1993;21(9):825-8.
38. Taylor SR, McLennan SM. The continental crust: Its composition and evolution; 1985.

Peer-review history:
The peer review history for this paper can be accessed here:
http://sciencedomain.org/review-history/18566